Croatian Society for Materials Protection

Metalurgija/Metallurgy

Vol. 65 No. 2 / 2026

Multi Response Modelling and Optimisation of Austempering Parameters on ADI Microstructure, Hardness and Fatigue Strength

Nikša Čatipović [1]*, Ivan Peko [2], Jure Krolo [1], Jelena Čulić-Viskota [3], Andrej Razumić [4]

https://doi.org/10.64486/m.65.2.4

[1] Faculty of Electrical Engineering, Mechanical Engineering and Naval Architecture, University of Split, Ruđera Boškovića 32, 21000 Split, Croatia; ncatipov@fesb.hr, jkrolo@fesb.hr
[2] Faculty of Science, University of Split, Ruđera Boškovića 33, 21000 Split, Croatia; ipeko@pmfst.hr
[3] Independent Researcher; jelena.culicviskota@gmail.com
[4] Department of Polytechnics, Dr. Franjo Tuđman Defense and Security University, Ilica 256b, Zagreb, Croatia; andrej.razumic@sois-ft.hr
* Correspondence: ncatipov@fesb.hr

Type of the Paper: Article
Received: September 11, 2025
***Accepted*:** November 6, 2025

Abstract: In this work, the influence of austempering temperature and time on the microstructure, hardness and fatigue strength of austempered ductile iron (ADI) is investigated. The experimental part was carried out on a total of eleven samples, nine of which were subjected to heat treatment at three temperatures (250 °C, 350 °C and 450 °C) and three time intervals (30 min, 75 min and 120 min). The tests included measurements of the fatigue strength, Vickers hardness and a microstructural analysis. The aim was to determine the optimum austempering parameters to achieve an ausferritic microstructure and improved mechanical properties. The results showed that austempering temperature had a significant effect on the properties of the treated samples, while austempering time did not show consistent statistical significance, although some samples deviated positively from the statistical model. The best result was obtained with the sample austempered at 350 °C for 120 minutes. Metallographic analysis confirmed the presence of an ausferritic microstructure, which contributed to the improved mechanical properties. The research highlights the importance of properly selecting austempering parameters to achieve an optimal combination of hardness and fatigue strength. Measured values were used to develop mathematical models which can be applied to predict analysed properties of ADI depending on austempering parameters.

Keywords: ADI; austempering parameters; hardness; fatigue; microstructural analysis; modelling

1. Introduction

Ductile iron represents an important material in today's foundry industry due to its good mechanical properties, favorable cost, and excellent machinability [1–3]. Thanks to these characteristics, it is widely used in various branches of industry, particularly in mechanical engineering and the automotive sector. Its primary microstructure, featuring spherically shaped graphite, contributes to toughness and fracture resistance.

Furthermore, it makes the material suitable for applications requiring impact and vibration resistance, as well as good ductility [4]. With the development of new technologies and industrial demands, interest in further improvement of the basic properties of these alloys has increased, with heat treatment playing a particularly important role. Of special significance is austempering, aimed at producing an ausferritic structure [5–6]. This process can significantly influence the hardness, durability, and material behavior under cyclic loading, as well as corrosion resistance [7]. The resulting microstructure after austempering is a consequence of the high silicon content in ductile iron, which limits the formation of carbides [8–11]. In addition to its energy and cost advantages, austempering also contributes to the improvement of mechanical properties: increased ductility, higher impact toughness, enhanced wear resistance, and improved fatigue strength. As previously mentioned, the fatigue strength of ductile iron can be significantly increased through appropriate heat treatment. Fatigue strength will be optimal if the matrix structure is homogeneous throughout the entire cross-section and free from defects. There are numerous microstructural factors that can reduce the fatigue strength of ductile iron, including increased nodule size, microporosity, eutectic carbides, slag, and other inclusions. These issues are particularly pronounced in massive castings [12–16]. ADI often possesses a clearly defined fatigue limit, which can be considerably higher than that of conventional ductile iron. This represents the stress level below which the material will not fail even after a very large number of cycles — typically 10^6 or more. Fracture generally initiates at the surface of the material under higher stresses and fewer cycles. At lower stresses and a higher number of cycles, fracture tends to occur within the material, due to crack initiation at graphite nodules. In comparison with steel, the fatigue strength of ADI is not solely dependent on tensile strength and hardness; in other words, the fatigue limit in ADI is not proportional to these two mechanical properties [17–21]. The amount and carbon content of retained austenite, graphite nodule size, nodularity, and the shape and size of ferrite significantly influence the material's performance under high-cycle fatigue loading [5]. In the study [6], X-ray diffraction analysis results showed that the amount of retained austenite in ADI decreases as the austempering temperature decreases. However, the higher toughness and ductility obtained at elevated austempering temperatures are attributed to the greater amounts of retained austenite [22]. The objective of this study was to examine the influence of temperature and time of austempering on the hardness, microstructure, and fatigue strength of austempered ductile iron. The experimental part of the work includes the heat treatment of samples, fatigue testing using a rotary bending machine, hardness measurements, and metallographic analysis. The obtained results were compared and analyzed using statistical software to identify the key parameters that most significantly affect the material properties [23, 24].

2. Materials and Methods

For the experimental part of the study, 11 ductile iron samples were prepared, but only 9 of them underwent the austempering heat treatment. The chemical composition of the used samples is shown in Table 1.

Table 1. Chemical composition of used ductile iron

Alloying element	C	Si	Mn	P	S	Mg	Cu	Cr
wt. / %	3.46	2.13	0.16	0.020	0.005	0.038	0.84	0.008

The experimental design was previously defined using the Design Expert software [25]. Input variables were selected as shown in Table 2, and the experimental plan designed by the software is shown in Table 3.

Table 2. Definition of input variables

Variable label	Input variable	Measuring unit	Lower level	Middle level	Higher level
A	Austempering temperature	°C	250	350	450
B	Austempering time	min	30	75	120

https://doi.org/10.64486/m.65.2.4

Table 3. Experimental plan

Sample id	Austempering temperature / °C	Austempering time / min
1	250	30
2	350	30
3	450	30
4	250	75
5	350	75
6	450	75
7	250	120
8	350	120
9	450	120

The initial Y test block, shown in Figure 1, was used for the preparation of samples according to the drawing shown in Figure 2. The Y block dimensions were 200 mm × 140 mm × 50 mm.

Figure 1. Initial Y block from which the samples were machined

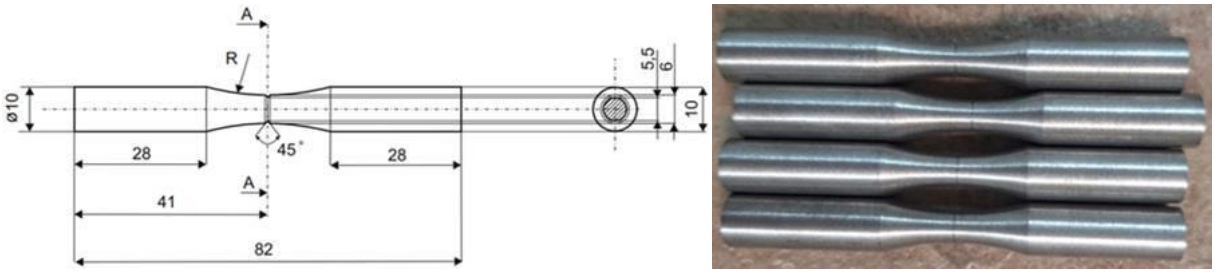

Figure 2. Drawing of the samples and finished machined samples

As shown in Figure 2, each sample featured a notch, or more precisely, a small central incision, to ensure that fracture would occur more rapidly during fatigue testing, thereby reducing the overall test duration. Additionally, the samples were designed specifically for the type of rotary fatigue testing machine used in the dynamic tests. The samples that were prepared, some of which are shown in Figure 2, were ready for the austempering and subsequent testing of fatigue strength, hardness, and microstructure. The experiments were conducted in the laboratories of the Faculty of Electrical Engineering, Mechanical Engineering, and Naval Architecture (FESB). The first stage of the experiment, heat treatment, began with the austenitization of the

https://doi.org/10.64486/m.65.2.4

samples in a laboratory furnace DEMITERM EASY 9. The furnace has a power rating of 3 kW and a maximum temperature of 1150 °C, which is measured using a Type K (NiCr–Ni) thermocouple with ± 2.2 °C accuracy.

As previously mentioned, 11 samples were prepared in total, but only 9 underwent heat treatment, while 2 samples were kept untreated to allow for a comparison between the as-cast and austempered conditions. The austenitization was carried out at a temperature of 850 °C for 45 minutes, in three groups of three samples each. After the austenitization holding period, each group of samples was subjected to austempering, performed in a JPA 6-600 furnace. This furnace has a power of 3.1 kW and a maximum temperature of 600 °C, measured with a Type K (NiCr–Ni) thermocouple with ± 2.2 °C accuracy.

The samples were directly quenched in the salt bath (AS 140) to obtain ADI. After completing the heat treatment, fatigue testing of ADI was performed. The fatigue strength was tested using a rotary bending fatigue testing machine.

The machine is of the rotary bending type, designed and built by the staff of the Department of Materials and Tribology in accordance with the relevant standards for rotary bending fatigue testing. Initially, one of the two untreated (as-cast) samples was tested to determine the appropriate load level for the subsequent tests on the austempered samples. The applied load on the first untreated sample was 50 N, but the sample fractured after only 2.9 seconds. It was concluded that the initial load was excessively high, so it was reduced to 20 N. The second untreated sample fractured after 1 minute and 17 seconds, and it was therefore decided that a 20 N load would be used for testing all remaining samples.

3. Results

3.1. Fatigue Strength

According to the obtained results, the untreated ductile iron exhibited moderate fatigue resistance, indicating a microstructure that is not sufficiently resistant to cyclic loading, yet still more resistant than the first group of heat-treated samples, as shown in Table 4.

Table 4. Time to fracture for ADI samples

Sample ID	1	2	3	4	5	6	7	8	9
Time to fracture / s	1.9	2.59	1.9	397.0	23.47	3 887.0	551.0	138.0	254.0

Samples 1–3 showed very low fatigue strength, even significantly lower than the untreated sample. The holding times in the salt bath were evidently insufficient for a stable microstructural transformation, resulting in a brittle microstructure with high fatigue sensitivity [26–28]. Austempering at 250 °C proved ineffective in this case, leading to property degradation rather than improvement.

Samples 4 and 5 demonstrated better fatigue resistance compared to the untreated material. However, sample 5 displayed a noticeable deviation. This may be due to insufficient transformation during heat treatment or minor variations in the austempering process that affected the final properties [29–31].

Sample 6 did not fracture, and the test was stopped manually at the time listed in Table 3. In sample 6, it is evident that a longer austempering time significantly increased fatigue strength, making it the best-performing sample after testing. Since no fracture occurred during the fatigue test, it can be concluded that this sample represents the optimal combination of temperature and time, i.e., the ideal austempering conditions for ADI to achieve the desired mechanical properties.

Samples 7–9 showed better fatigue strength compared to samples 1–3. Based on the rotational speed of the rotary bending fatigue testing machine (2 700 rpm) and the time to fracture for each sample, the number of revolutions at the moment of fracture was calculated and is listed in Table 5.

https://doi.org/10.64486/m.65.2.4

Table 5. Number of RPM until fracture for ADI samples

Sample ID	RPM to fracture
Original_test 1	130.5
Original_test 2	3 465.0
1	85.5
2	116.6
3	85.5
4	17 865.0
5	1 056.2
6	174 915.0
7	24 795.0
8	6 210.0
9	8 730.0

For sample 6, the number of revolutions corresponds to the point at which the fatigue test was stopped. Samples 7–9 exhibited inconsistent results. Although Sample 7 showed good fatigue strength, a further increase in holding time did not improve but rather degraded the fatigue performance. The time to fracture was considerably better than in the first group of samples; however, the austempering temperature of 450 °C was found to be non-optimal, and prolonged holding further compromised the structural stability. The reason for this is decomposition of the ausferrite phase into ferrite and carbides which lead to degradation of mechanical properties. The results from Table 5 were imported into the Design Expert software, and the effect of austempering heat treatment parameters on the number of cycles to fracture was analysed to determine the dominant factor influencing fatigue life. The Analysis of Variance (ANOVA) results, shown in Table 6, indicated that the model was statistically significant ($F = 28.17$, $p = 0.0034$), confirming that at least one of the tested factors had a significant effect on the number of cycles to failure. The analysis further revealed that the isothermal temperature (Factor A) had a statistically significant influence ($p = 0.0012$), meaning that changes in temperature substantially affected the material's durability under cyclic loading.

Table 6. ANOVA analysis for fatigue strength

Source	Sum of Squares	df	Mean Square	*F*-value	*p*-value	
Model	0.0167	4	0.0042	28.17	0.0034	significant
A – austempering temperature	0.0167	2	0.0083	56.18	0.0012	significant
B – austempering time	0.0000	2	0.0000	0.1569	0.8598	
Residual	0.0006	4	0.0001			
Cor Tota	0.0173	8				
Std. Dev.	0.0122					
Mean	0.0421					
C.V. %	28.90					
R^2	0.9657					
Adjusted R^2	0.9314					
Predicted R^2	0.8264					
Adeq. Precision	10.7949					

https://doi.org/10.64486/m.65.2.4

Conversely, the austempering time (Factor B) was not statistically significant (p = 0.8598), implying that the duration of holding at a given temperature did not consistently affect the number of cycles to fracture. Although statistical results suggested that the holding time was not a significant factor, Sample 6 experimentally achieved the best fatigue performance in the entire study. This indicates that a combination of moderate temperature and longer holding time can lead to very favourable material properties, which has been supported with previous research [19]. The model quality statistics demonstrated how accurately and reliably the mathematical model described the data and predicted outcomes. The coefficient of determination (R^2) indicates how well the model explains variations in the results. In this case, the model explained the variations very well, with an R^2 value of 96.57 %. The adjusted R^2, which accounts for the number of factors in the model, showed only a small difference from the regular R^2 value, indicating that the model was not overfitted with unnecessary terms. The predicted R^2, representing the model's ability to forecast new data not included in the analysis, was 85.64 %, confirming that the predictive capability of the model was reliable. The Adeq Precision value, which measures the signal-to-noise ratio, was 10.8, well above the recommended threshold of 4—demonstrating a strong model signal relative to random variation. In summary, the statistical evaluation confirmed that the developed model is accurate, robust, and reliable for describing the observed data and for making future predictions regarding the influence of austempering parameters on the fatigue life of ADI. The coefficients of the regression model indicate how the response variable, the number of cycles to fracture, changes when a given factor varies from level –1 to +1. From Table 7, it can be observed that the highest temperature (A_{high}), the medium temperature (A_{low}), and the factors B_{high} and B_{low} (representing isothermal holding times) have negligible effects.

Table 7. Coefficients for coded factors

Term	Coefficient Estimate	df	Standard Error	95% CI Low	95% CI High
Intercept	0.0421	1	0.0041	0.0309	0.0534
A_{high}	0.0608	1	0.0057	0.0449	0.0768
A_{low}	−0.0286	1	0.0057	−0.0445	−0.0127
B_{high}	−0.0015	1	0.0057	−0.0174	0.0145
B_{low}	0.0032	1	0.0057	−0.0127	0.0192

Their influence is minimal because there is no statistically clear correlation—that is, the austempering time does not affect the response consistently across all cases, as previously discussed. In contrast, the A_{high} factor (high temperature) significantly increases the number of cycles, improving the material's fatigue strength, whereas the A_{low} factor slightly decreases fatigue resistance compared to the baseline condition. The software also generated a final regression equation (1) in coded values.

$$\frac{1}{\sqrt{(RPMs\ to\ fracture)}} = 0{,}0421 + 0{,}0608 \cdot \mathrm{A}_{\mathrm{high}} - 0{,}0286 \cdot A_{\mathrm{low}} - 0{,}0015 \cdot B_{\mathrm{high}} + 0{,}0032 \cdot B_{low} \quad (1)$$

This equation can be used for rapid response prediction when the coded factor values are known and calculated, as well as for comparing the relative influence of each factor. Therefore, if additional samples or parameter adjustments are planned, it is not necessary to immediately conduct experimental testing. Instead, the factor values can first be input into the model to obtain an estimated fatigue strength, after which a decision can be made on whether to proceed with physical testing. The graphical representation of the results, shown in Figure 3, corresponds with inverse sqrt transformation of the model, and not with measured values themselves.

https://doi.org/10.64486/m.65.2.4

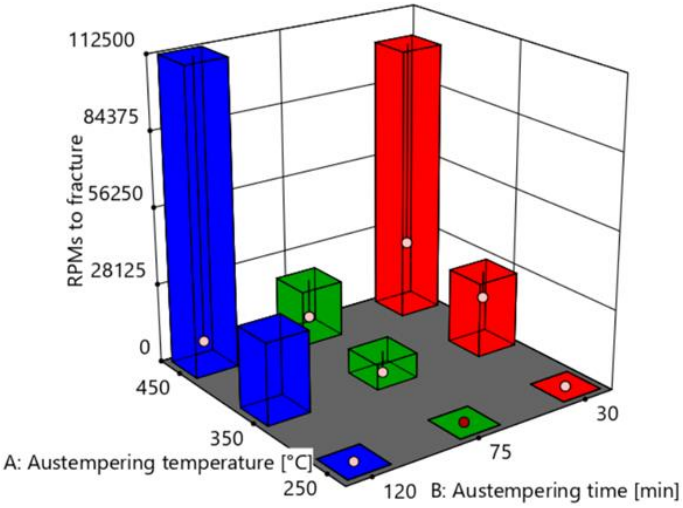

Figure 3. Graphical representation of fatigue strength results

However, this value does not align with statistical expectations, suggesting that this sample may represent a local optimum within the range of heat treatment parameters. As mentioned earlier, the model does not recognize this as a general rule but rather as a potential exception. This result suggests that austempering time may indeed have a notable influence, but only in combination with a specific temperature, a phenomenon known as an interaction effect. Since this effect was not included in the original model, it is recommended to extend the experimental design with additional data points around 350 °C and 120 minutes, and to include interaction terms in the regression model to verify this hypothesis, which will be explored in future work.

3.2. Hardness

After the fatigue strength testing, the hardness of the ADI samples was evaluated using the Vickers method. Prior to testing, the samples were ground using a Handiment Grinder with a 320-grit water-based abrasive track. The Vickers hardness test involved indenting the surface of the material with a diamond pyramid-shaped indenter under a specific load of 10 kP with measurement accuracy of ± 2 %. After indentation, a square-shaped impression was formed on the surface, and its diagonals were measured under a microscope. Based on the mean diagonal length of the indentation and the applied load, the Vickers hardness (HV10) of the material was calculated. The hardness results for all tested samples are presented in Tables 8.

Table 8. Hardness results for ADI samples

Sample ID	Hardness / HV10				
	1. measurement	2. measurement	3. measurement	Mean	Std. Dev.
Original	232	230	230	230.7	1.16
1	498	498	498	498.0	0.00
2	327	333	330	330.0	3.00
3	276	283	276	278.3	4.04
4	468	468	473	469.7	2.89
5	351	342	342	345.0	5.20
6	274	281	279	278.0	3.61
7	464	473	483	473.3	9.50
8	348	345	354	349.0	4.58
9	283	281	281	281.7	1.15

All samples were subjected to three measurements to obtain a more accurate average hardness value. The hardness of the untreated (as-cast) sample served as the baseline reference value for all heat-treated samples. Observing the mean value, it is evident that the hardness is low, which is typical for ductile iron without heat

https://doi.org/10.64486/m.65.2.4

treatment. This clearly demonstrates the significant effect of austempering heat treatment on the material's hardness. Although the untreated sample exhibits the lowest hardness, it shows greater fatigue strength than all samples austempered for 30 minutes. This confirms that high hardness does not necessarily correlate with higher fatigue strength. In fact, it often implies lower resistance to dynamic loading.

From Table 8, it is evident that after 30 minutes of austempering, the samples achieved the highest hardness values in the entire dataset—nearly double those of the untreated sample. This indicates a very efficient hardening process at this temperature over a short duration. However, in Sample 4, a noticeable drop in hardness of approximately 30 HV was recorded, suggesting that extended holding at this temperature reduces hardness, likely due to microstructural changes that slow down the hardening effect. In Sample 7, a slight increase in hardness was observed, but the value did not return to the initial peak recorded for Sample 1. Therefore, short-term heat treatment at 250 °C results in high hardness, but the outcome is highly sensitive to holding time. When compared with the results from the fatigue testing, which showed low fatigue strength for samples austempered at 250 °C, it can be concluded that this group demonstrates pronounced brittleness, confirming the typical inverse relationship between hardness and fatigue strength in ADI materials. Observing Table 8, it is evident that the hardness values are higher than those of the untreated sample, but lower than the values obtained for austempering at 250 °C. A gradual and stable increase in hardness with time is noticeable. The increase between 30 minutes and 75 minutes amounts to 15 HV, while the difference between 75 minutes and 120 minutes is only 1.4 HV, indicating that a nearly stable state was reached after 75 minutes. Since sample 5 fractured early in the previous fatigue test, it is clear that fracture resistance in this temperature range does not develop solely as a function of increasing hardness but the austempering time also plays a crucial role. Therefore, samples austempered at 350 °C represent the most favourable temperature range for achieving uniform and stable hardness without significant fluctuations. This confirms that at higher austempering temperatures, the material's behaviour becomes less dependent on hardness and more influenced by the development of internal resistance to crack propagation under cyclic loading. Obtained results were entered into the Design Expert software to establish a reliable mathematical model and identify which parameters most significantly influence hardness changes. The statistical analysis results (ANOVA), shown in Table 9, indicate that the overall model is statistically significant, meaning that the selected parameters, temperature and time, have a substantial impact on hardness.

Table 9. ANOVA analysis for hardness

Source	Sum of Squares	df	Mean Square	*F*-value	*p*-value	
Model	63 930.30	4	15 982.61	104.16	0.0003	significant
A – austempering temperature	63 896.89	2	31 948.44	208.21	< 0.0001	significant
B – austempering time	33.56	2	16.78	0.1093	0.8990	
Residual	613.78	4	153.44			
Cor Tota	64 544.22	8				
Std. Dev.	12.39					
Mean	366.56					
C.V. %	3.38					
R^2	0.9905					
Adjusted R^2	0.9810					
Predicted R^2	0.9519					
Adeq. Precision	22.3115					

https://doi.org/10.64486/m.65.2.4

The austempering temperature (Factor A) showed a very strong effect, with an *F*-value of 208.21 and a p-value < 0.0001, confirming that temperature variation strongly affects hardness. The austempering time (Factor B), on the other hand, again showed a negligible influence, with $F = 0.11$ and $p = 0.8990$, indicating that changes in heat treatment duration do not significantly impact hardness. The model quality metrics once again confirmed that the regression model is highly precise and can be reliably used for predicting hardness in new samples without additional testing. The model coefficients in coded values, shown in Table 10, indicate that the highest hardness is achieved at the maximum experimental temperature (450 °C), corresponding to Factor A_{high}.

Table 10. Coefficients for coded factors

Term	Coefficient Estimate	df	Standard Error	95% CI Low	95% CI High
Intercept	366.56	1	4.13	355.09	378.02
A_{high}	113.78	1	5.84	97.56	129.99
A_{low}	−26.22	1	5.84	−42.44	−10.01
B_{high}	2.11	1	5.84	−14.10	18.32
B_{low}	−2.56	1	5.84	−18.77	13.66

The medium temperature (A_{low}) slightly reduces hardness, while the *B* factors (time) exhibit minimal, practically negligible influence. The model equation (2) uses coded values, allowing hardness prediction for different combinations of process conditions.

$$HV10 = 366{,}56 + 113{,}78 \cdot \mathrm{A}_{high} - 26{,}22 \cdot \mathrm{A}_{low} + 2{,}11 \cdot B_{high} - 2{,}56 \cdot B_{low} \quad (2)$$

The graphical representation in Figure 4 clearly shows that the highest hardness belongs to the samples austempered at lowest temperatures, while with the increase of austempering temperature hardness drops. The graph confirms that time has no significant effect, as the bars corresponding to the same temperature are similar regardless of holding duration.

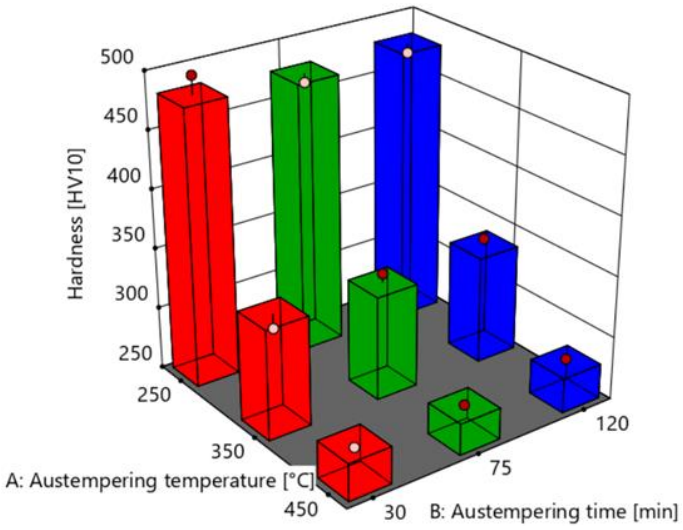

Figure 4. Graphical representation of hardness results

3.3. Microstructure

In the final stage of the experiment, a metallographic analysis was carried out. Prior to the analysis, the samples were prepared and polished using a MINITECH 250 SP1 manual grinding and polishing machine. This device uses discs with diameters ranging from 200 mm to 250 mm, features a 750 W motor, and includes a touchscreen interface for controlling and programming process parameters such as time, speed, and rotation direction.

https://doi.org/10.64486/m.65.2.4

Polishing cloths with a 250 mm diameter and grit sizes P180, P320, P600, and P1200 were used, the TOP, RAM, NT, and SUPRA 5 models, respectively. During polishing, monocrystalline diamond suspensions and a lubricant were applied. The diamond particle sizes used were 9 μm, 3 μm, 1 μm, and 0.03 μm, applied sequentially from left to right, corresponding to the increasing fineness of the polishing cloths. Once the sample surfaces were properly prepared, the etching phase followed. This step is essential for revealing the microstructure, allowing for detailed microscopic observation. A stereo upright optical microscope (OPTON Axioskop) was used, connected to a computer monitor via a Dino Eye eyepiece camera.

The DinoCapture 2.0 software was employed for image acquisition and analysis. For etching, a 3 % nital solution (5 ml), consisting of nitric acid in ethyl alcohol, was used. The reagent was applied by placing three drops onto the sample surface, allowing a brief reaction period, after which the sample was rinsed, dried, and ready for metallographic examination. The initial etching time was planned to be 10 seconds, but the metallography of the untreated sample revealed that the reagent over-etched the surface, so the reaction time was reduced to 5 seconds. The metallographic analysis of that sample was then repeated to achieve more accurate and representative results. The metallographic images shown in Figure 5 illustrate the microstructure of the untreated sample as well as the samples that underwent heat treatment and austempering. For all samples, metallographic analysis was performed at magnifications of 100x, 200x, and 500x, but for clarity and easier comparison among the ADI samples, only the 200x images are presented.

1. Microstructures of original sample: a) 100x, b) 200x, c) 500x

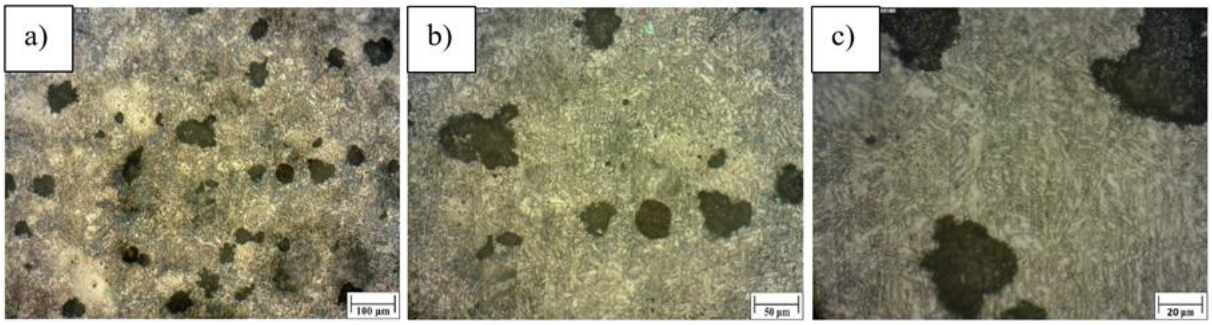

2. Microstructures of ADI samples at 250 °C: a) 30 min, b) 75 min, c) 120 min

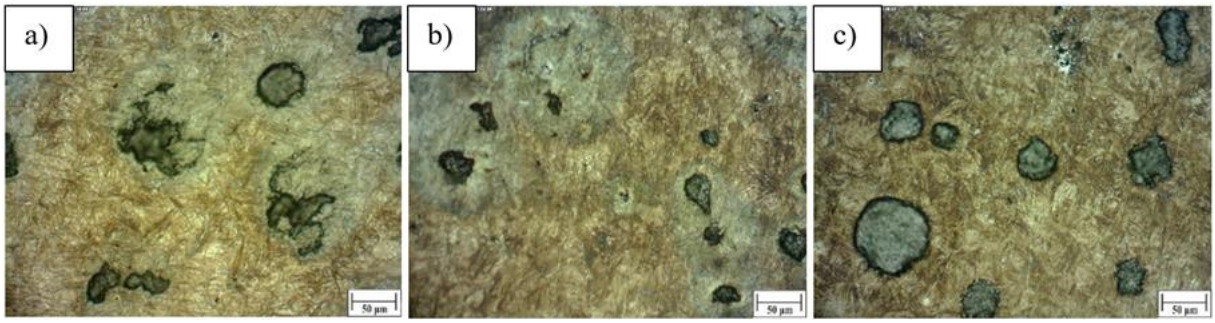

3. Microstructures of ADI samples at 350 °C: a) 30 min, b) 75 min, c) 120 min

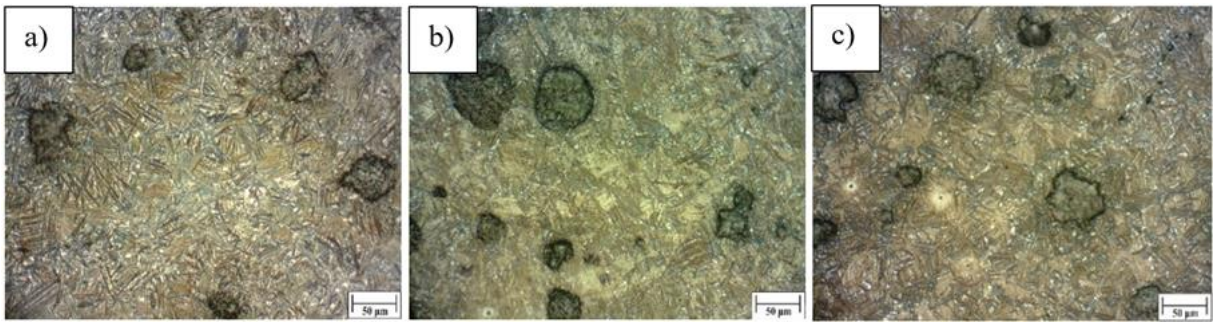

https://doi.org/10.64486/m.65.2.4

4. Microstructures of ADI samples at 450 °C: a) 30 min, b) 75 min, c) 120 min

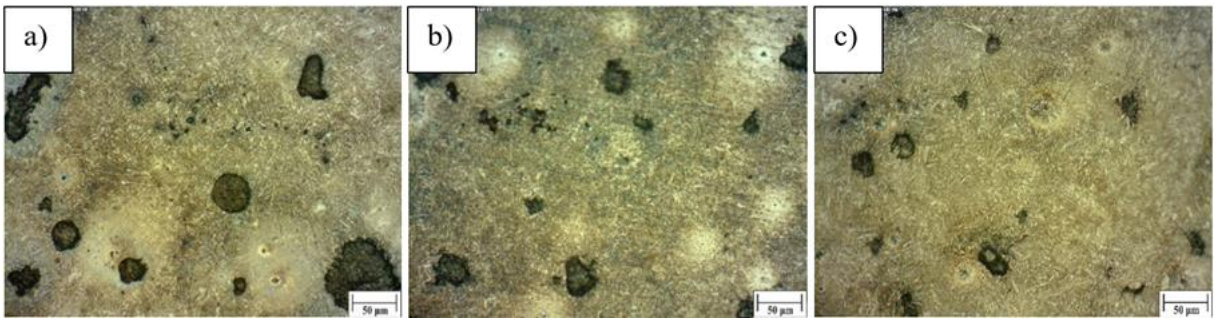

Figure 5. Obtained microstructures of untreated sample and ADI samples

4. Discussion

Analyzing the microstructure of the untreated sample, spheroidal graphite nodules are clearly visible. These are uniformly distributed throughout the matrix, without signs of deformation, indicating well-controlled casting conditions and successful graphite spheroidization through magnesium (Mg) treatment. The graphite nodules have well-defined edges, and their size varies, though most are of medium to fine grain size, demonstrating good homogeneity of the casting. It is evident that the matrix of the untreated sample consists of a ferrite–pearlite structure. The ferrite phase appears as the lighter regions, typically forming halos around the graphite nodules. These ferritic halos result from carbon diffusion during the rapid cooling of the molten material. Such localized phase transformation enhances impact and fracture resistance, as it helps relieve stresses around inclusions. Conversely, pearlite occupies the regions between ferritic zones and is recognizable by its lamellar morphology and darker appearance under the microscope. At 500× magnification, pearlite lamellae were clearly visible, confirming the absence of bainite or martensite, which would display distinct morphologies and different etching responses. The microstructure of the untreated sample confirms findings from the hardness and fatigue experiments. Its low hardness stems from the ferrite–pearlite composition. Ferrite is very soft, while pearlite contributes only modestly to overall hardness. Higher fatigue strength of the untreated material compared to samples austempered at 250 °C is due to the ductility of ferrite, which can plastically deform and absorb energy prior to fracture, as well as the moderate strength of pearlite. The spherical shape of the graphite nodules also improves mechanical properties, since rounded inclusions act as weaker stress concentrators than sharp or irregular ones.

In Figure 5.2.a), it can be observed that the graphite nodules remained clearly visible and unaffected by the heat treatment, meaning they have retained their shape and uniform distribution without signs of degradation, confirming that the austempering process targeted only the metallic matrix. This early stage of austempering transformation (30 minutes) produced a lower ausferrite microstructure, confirmed in previous work [32]. The lower ausferrite explains the high hardness values, which are significantly higher than those of the as-cast material. The microstructure exhibits a fine, densely packed needle-like morphology, with ferritic needles rapidly formed within the previously austenitized matrix. Such a structure provides excellent hardness and wear resistance, but results in low toughness and poor fatigue strength. In Figure 5.2.b), more pronounced transition zones can be seen around the graphite nodules. These nodules remain inactive elements within the microstructure, while the surrounding matrix has transformed into a needle-like structure that is less dense and less ordered than in the previous sample. Compared to the earlier stage, the ausferritic structure evolved further, with upper ausferrite beginning to dominate. The needles of ferrite and stabilized austenite appear thicker and longer, reflecting the extended transformation time. The ferrite becomes more interwoven, and the proportion of retained austenite increases, since longer austempering time allows for carbon diffusion. At this stage, prolonged austempering time at this temperature leads to partial relaxation of internal stresses and a slight improvement in ductility. Technically, the sample offers better impact resistance while maintaining high hardness but is still unsuitable for components subjected to cyclic loading. The analysis of Figure 5.2.c) again confirms the good preservation and distribution of graphite nodules, though some micro segregation around

https://doi.org/10.64486/m.65.2.4

them is possible. No coarse pearlite zones or fracture traces were detected. The matrix remains dominated by ausferrite, but with an even more pronounced upper ausferritic structure and needle-like ferrite. The needles are longer and more sparsely distributed than in the 75 minute sample. A higher proportion of retained austenite, visible as darker regions, indicates microstructural stabilization. No martensite, pearlite, or carbide phases were observed; the zones are clean, smooth, and well-connected, showing a stable microstructure. However, when compared with fatigue strength and hardness test results, it is evident that longer austempering time at 250 °C does not improve fatigue strength, but in fact, it may lead to local imbalance in the microstructure. This behaviour suggests that toughness, although not directly measured, was not enhanced and may have slightly degraded, which correlates with results presented in [18]. The resulting microstructure remains ideal for high hardness but does not ensure satisfactory dynamic performance under cyclic or impact loads.

In the second series of metallographic images shown in Figure 5.3.a), the structure consists of early-stage upper ausferrite. Unlike lower ausferrite, which provides higher hardness and strength, upper ausferrite results in greater ductility but lower hardness. It is characterized by needle-like ferrite, clearly visible throughout most of the matrix. The needles are thin, sharply defined, and linearly oriented, but they are more sparsely distributed, and the matrix appears darker, indicating a significant amount of retained austenite. The phase boundaries are clear, but the structure remains partially transformed. This is due to the slower transformation kinetics at 350 °C compared to 250 °C. Within the 30 minutes duration, there is insufficient time for complete transformation of austenite to ferrite. Carbon diffusion has begun but is not yet extensive enough to stabilize a larger portion of austenite, resulting in a high retained austenite content. The graphite nodules remain uniformly distributed and free of stress concentrations. A sample with this type of microstructure exhibits balanced mechanical properties: the coarser and less strained ausferritic network allows the material to absorb energy before fracture, offering a good initial balance between hardness and fatigue strength. The 75 minute heat treatment allowed for a full development of upper ausferrite, meaning that most of the austenite transformed into ferrite. In Figure 5.3.b), the matrix shows densely distributed, thick ferritic needles that interweave to form a stable network. Some localized stresses may occur around graphite nodules. The lighter and more homogeneous appearance compared to the 30 minute sample indicates dominant ferritic content. The darker interphase areas remain, but retained austenite appears only as a dispersed secondary phase. This sample exhibited an increase in hardness accompanied by a lower fatigue strength, which can be attributed to the more rigid, mesh-like structure where stress localizes around graphite particles, promoting crack initiation. The microstructure suggests that the ausferrite evolved into a stronger but less deformable phase network. Thus, while mechanical strength increased, toughness and fatigue resistance decreased, indicating that strength was gained at the expense of ductility. The longest austempering time at 350 °C, represented in Figure 5.3.c), resulted in a fully transformed matrix with stabilized retained austenite, indicating microstructural maturity. The matrix consists of a branched network of needle-like ferrite intertwined with stable retained austenite. The needles appear broad and partially rounded, merging with the austenitic phase—making the phase boundaries difficult to distinguish under the microscope. The overall structure appears relaxed, with stable graphite–matrix interactions. The dark interphase regions represent the retained austenite, now expanded and stabilized, forming broad dark zones. Although the contrast is lower, the structure is fully developed and coherent. Owing to this coarser yet uniformly distributed ausferritic structure, the sample demonstrates exceptional fatigue strength while maintaining high hardness, providing excellent mechanical stability. This regime yielded the best overall performance, combining high hardness, structural stability, and outstanding dynamic load resistance.

At higher austempering temperatures of 450 °C, the transformation rate increases, but it also promotes the formation of a coarser and less compact structure, as seen in Figure 5.4.a). The structure corresponds to an early-stage upper ausferrite with some retained austenite, but not yet fully homogeneous. The matrix appears predominantly light, with clearly visible ferritic needles that are thicker, shorter, and widely spaced. The phase boundary between ferrite and austenite is less distinct, which is typical at higher temperatures. Ferrite forms rapidly but does not completely replace austenite, leaving residual untransformed austenite. The graphite nodules remain well-shaped but unevenly distributed. As previously established, the hardness of samples in this group is the lowest, consistent with the coarser, less compact ausferritic matrix. This type of structure allows for greater deformability and lower internal stress, thereby prolonging service life under cyclic loading. The

https://doi.org/10.64486/m.65.2.4

combination of time and temperature used for the sample in Figure 5.4.b) enabled greater carbon diffusion into austenite and increased phase stabilization, leading to the development of upper ausferrite. The matrix appears uniformly bright with faint darker areas, suggesting the presence of ferrite with a higher proportion of stable austenite. The ferritic needles are relatively wide, interwoven yet separated, with rounded edges and poorly defined phase boundaries. Retained austenite fills the spaces between ferritic regions, forming a stable interconnected network. However, fatigue strength testing revealed that this sample fractured much sooner than the 30 minute sample, despite having nearly identical hardness. This suggests that prolonged exposure at high temperature may cause microstructural incoherence, reducing the material's ability to transmit and absorb cyclic stresses. The microstructure indicates a loss of uniform ausferritic texture, which facilitates faster crack propagation under fatigue loading. Consequently, these austempering parameters provide weaker overall performance compared to the previous one. In the final sample, shown in Figure 5.4.c), the matrix appears bright and homogeneous. The graphite nodules appear slightly smaller and moderately uniform in distribution. This may be due to reduced contrast between the matrix and graphite, or to extended carbon diffusion at the boundaries into the surrounding austenite. The shape and distribution of the nodules remain regular, confirming that the thermal conditions did not cause graphite degradation. The ferritic needles are broad, curved, and poorly defined, seemingly blending into the retained austenite. The phase boundaries are highly subdued, as expected in a mature, thermodynamically stable microstructure. Retained austenite appears in large, dark interconnected zones, no longer as isolated pockets but as a continuous linking phase between ferritic networks.

5. Conclusions

Based on the analysis of the conducted experiments, it can be concluded that the austempering temperature has a significant and direct influence on the microstructural evolution of austempered ductile iron and consequently on its mechanical properties, such as hardness and fatigue strength. Among the three analysed temperatures, the treatment performed at 350 °C yielded the best results in terms of material durability under cyclic loading, while the lower (250 °C) and higher (450 °C) temperature ranges produced less stable or less favourable outcomes. In particular, the sample treated at 350 °C for 120 minutes did not fail during fatigue testing, demonstrating exceptional resistance to cyclic stresses. The austempering time did not show a consistent statistical effect on material properties; however, the experimental data and previous research suggest that under certain conditions, holding time may have a positive interaction effect with temperature. It was also confirmed that high hardness does not necessarily correlate with improved fatigue resistance, as evidenced by the 250 °C samples, which exhibited the highest hardness but the lowest fatigue strength. The metallographic analysis provided a detailed insight into the microstructure of each sample and confirmed the formation of an ausferritic structure in those samples that demonstrated superior fatigue performance. Based on the obtained data, a statistical model was developed, enabling the prediction of material behaviour under specific heat treatment parameters. This model can serve as a foundation for process optimization in industrial applications. This study clearly demonstrates that the application of a properly designed heat treatment can significantly improve the dynamic performance of ADI. As a guideline for further research, it is recommended to expand the experimental study to include additional austempering temperature–time combinations, as well as to incorporate other influential factors such as chemical composition, cooling rate, and sample geometry, with the goal of achieving complete process optimization and broader applicability in technical and industrial practice.

In conclusion, this study has demonstrated that through the optimization of austempering parameters, ductile iron can be transformed into a high-performance engineering material with a superior combination of strength, ductility, and fatigue strength. The results contribute to a deeper understanding of the structure–property relationship in ADI and provide practical guidelines for its broader application in modern engineering practice.

https://doi.org/10.64486/m.65.2.4

References

[1] C. Labercque and M. Gagne, *Ductile Iron—Fifty Years of Continued Development.* Sorel-Tracy, QC, Canada: Rio Tinto Iron & Titanium, 1998.

[2] ASTM International, *Standard Specification for Austempered Ductile Iron Castings,* ASTM A897/A897M-22, 2022.

[3] M. Y. Abdellah et al., "Mechanical Properties and Fracture Toughness Prediction of Ductile Cast Iron under Thermomechanical Treatment," *Metals*, vol. 14, no. 352, 2024, https://doi.org/10.3390/met14030352

[4] G. Behera, "Effect of Copper on the Properties of Austempered Ductile Iron Castings," B.S. thesis, Dept. Metallurgical and Materials Engineering, National Institute of Technology, Rourkela, India, 2012.

[5] T. Sarkar, "Analysis of Mechanical Properties of Austempered Ductile Iron Weld Joints Using Developed Electrode," in *Recent Advancements in the Metallurgical Engineering and Electrodeposition*, D. S. Robinson, Ed. London, U.K.: IntechOpen, 2019, https://doi.org/10.5772/intechopen.84763

[6] C.-K. Lin, P.-K. Lai, and T.-S. Shih, "Influence of microstructure on the fatigue properties of austempered ductile irons," *International Journal of Fatigue*, vol. 18, no. 5, pp. 297–307, Jul. 1996.

[7] L. Vrsalović, N. Čatipović, S. Gudić, and S. Kožuh, "Beneficial Effect of Cu Content and Austempering Parameters on the Hardness and Corrosion Properties of Austempered Ductile Iron (ADI)," *Facta Universitatis, Series: Mechanical Engineering*, vol. 23, no. 1, pp. 33–47, 2025, https://doi.org/10.22190/FUME220106018V

[8] N. Čatipović et al., "Influence of a Novel Double Tempering Process on the Microstructure and Mechanical Properties of Cu-Alloyed Austempered Ductile Iron," *Crystals*, vol. 13, no. 1359, 2023, https://doi.org/10.3390/cryst13091359

[9] Pine Pacific, "Global Casting Production Trend and Conclusion in 2014," *Pine Pacific Website*, 2014. [Online]. Available: https://www.pinepacific.com/news_detail.php?idnews=93 [Accessed: Aug. 2, 2025].

[10] R. Bendikiene et al., "Influence of Austempering Temperatures on the Microstructure and Mechanical Properties of Austempered Ductile Cast Iron," *Metals*, vol. 11, no. 967, 2021, https://doi.org/10.3390/met11060967

[11] O. J. Akinribide et al., "A Review on Heat Treatment of Cast Iron: Phase Evolution and Mechanical Characterization," *Materials*, vol. 15, no. 7109, 2022, https://doi.org/10.3390/ma15207109

[12] L. Sidjanin and R. E. Smallman, "Metallography of bainitic transformation in austempered ductile iron," *Materials Science and Technology*, vol. 8, pp. 1095–1103, 1992, https://doi.org/10.1179/mst.1992.8.12.1095

[13] R. Elliot, "The role of research in promoting austempered ductile iron," *Heat Treatment of Metals*, vol. 24, pp. 55–59, 1997.

[14] M. Landesberger et al., "Phase Transition Kinetics in Austempered Ductile Iron (ADI) with Regard to Mo Content," *Materials*, vol. 13, no. 5266, 2020, https://doi.org/10.3390/ma13225266

[15] E. Tyrała et al., "Evaluation of Volume Fraction of Austenite in Austempering Process of Austempered Ductile Iron," *Metals*, vol. 9, no. 893, 2019, https://doi.org/10.3390/met9080893

[16] H. Chandler, *Heat Treaters Guide: Practices and Procedures for Irons and Steels*, 2nd ed. West Conshohocken, PA, USA: ASTM International, 1994.

[17] J. Bai et al., "Microstructures and Mechanical Properties of Ductile Cast Iron with Different Crystallizer Inner Diameters," *Crystals*, vol. 12, no. 413, 2022, https://doi.org/10.3390/cryst12030413

[18] C.-H. Hsu, C.-Y. Lin, and W.-S. You, "Microstructure and Dry/Wet Tribological Behaviors of 1% Cu-Alloyed Austempered Ductile Iron," *Materials*, vol. 16, no. 2284, 2023, https://doi.org/10.3390/ma16062284

[19] A. Sharma, K. K. Singh, and G. K. Gupta, "Study on the Effects of Austempering Variables and Copper Addition on Mechanical Properties of Austempered Ductile Iron," in *Proc. 6th Int. & 27th All India Manufacturing Technology, Design and Research Conf.*, Pune, India, Dec. 16–18, 2016.

[20] B. Mrzygłód et al., "Characteristics of ADI ductile cast iron with single addition of 1.56% Ni," *Archives of Metallurgy and Materials*, vol. 62, no. 4, pp. 2273–2280, 2017, https://doi.org/10.1515/amm-2017-0335

[21] Croatian Standards Institute, *EN ISO 148-1:2012 – Metallic Materials—Charpy Pendulum Impact Test—Part 1: Test Method*, Zagreb, Croatia, 2010. [Online]. Available: https://repozitorij.hzn.hr/norm/HRN+EN+ISO+148-1:2012 [Accessed: Aug. 2, 2025].

[22] N. Čatipović et al., "Multi Response Modelling and Optimisation of Copper Content and Heat Treatment Parameters of ADI Alloys by Combined Regression Grey-Fuzzy Approach," *Metals*, vol. 14, no. 735, 2024, https://doi.org/10.3390/met14060735

https://doi.org/10.64486/m.65.2.4

[23] H. Krawiec et al., "Influence of heat treatment parameters of austempered ductile iron on the microstructure, corrosion and tribological properties," *Materials*, vol. 16, no. 3, p. 1256, 2023, https://doi.org/10.3390/ma16114107

[24] Croatian Standards Institute, *EN 1563:2018 – Founding—Spheroidal Graphite Cast Irons,* Zagreb, Croatia, 2018. [Online]. Available: https://repozitorij.hzn.hr/norm/HRN+EN+1563:2018 [Accessed: Aug. 2, 2025].

[25] State-Ease, *Design Expert 13 Software,* 2025. [Online]. Available: https://www.statease.com/training/quick-start-resources/ [Accessed: Aug. 2, 2025].

[26] S. M. Banavasi, R. K. Singh, and P. S. Naik, "A Review on Design and Fabrication of Fatigue Testing Machine," *International Journal of Novel Research and Development,* vol. 3, no. 5, pp. 5–13, May 2018.

[27] M. Petrenec *et al.*, "Analysis of fatigue crack initiation in cycled austempered ductile cast irons," *Procedia Engineering,* vol. 2, no. 2, pp. 2337–2346, 2010, https://doi.org/10.1016/j.proeng.2010.03.250

[28] P. Hübner *et al.*, "Low cycle fatigue of ADI: Observations on cyclic plasticity and crack initiation," *Materials Science and Engineering A,* vol. 498, no. 1–2, pp. 94–101, Dec. 2008.

[29] R. O. Ritchie and J. F. Knott, "Mechanisms of fatigue-crack propagation in ductile and brittle solids," *Journal of Engineering Materials and Technology,* vol. 95, no. 4, pp. 415–422, Oct. 1973, https://doi.org/10.1023/A:1018655917051

[30] J. A. Bannantine, J. J. Comer, and J. L. Handrock, *Fundamentals of Metal Fatigue Analysis.* Englewood Cliffs, NJ: Prentice Hall, 1990.

[31] D. A. Porter and K. E. Easterling, *Phase Transformations in Metals and Alloys,* 2nd ed. London, U.K.: Chapman & Hall, 1992.

[32] N. Čatipović, D. Živković, Z. Dadić, and P. Ljumović, "Effect of Copper and Heat Treatment on Microstructure of Austempered Ductile Iron," *Transactions of the Indian Institute of Metals,* vol. 74, pp. 1455–1468, 2021, https://doi.org/10.1007/s12666-021-02225-6

https://doi.org/10.64486/m.65.2.4